

Singlet Fission in a Binary System: Effect of Structural Changes and Temperature

Marina Gerhard,* Julian Hausch, Nico Hofeditz, Jona Bredehöft, Katharina Broch, and Frank Schreiber*



Cite This: *J. Phys. Chem. C* 2024, 128, 13926–13936



Read Online

ACCESS |



Metrics & More

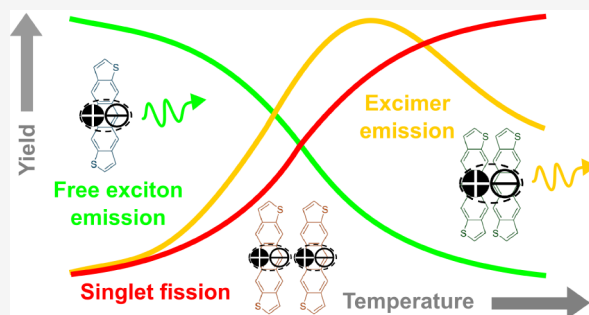


Article Recommendations



Supporting Information

ABSTRACT: Singlet fission is a promising mechanism to boost the performance of solar cells. In order to establish efficient singlet fission, it is essential to understand and control competing decay channels such as the occupation of trap states and the formation of excimers, for which the local ordering of the molecules plays an essential role. To systematically explore effects of molecular packing, a promising strategy is to blend the material of interest with another molecular compound. In the present study, we investigate binary thin films of anthradithiophene (ADT) and the high bandgap molecule hexaphenylbenzene with different compound ratios. By utilizing X-ray diffraction techniques and steady state optical spectroscopy, we identify a phase separating regime where the structural quality can be systematically tuned. Combining these subtle structural modifications with time-resolved and temperature-dependent photoluminescence spectroscopy allows us to independently manipulate the energetic landscape and thermal activation of kinetic processes. Eventually, our findings enable us to refine current models of the excited-state photophysics of ADT, suggesting that singlet fission critically depends on the number of neighboring ADT molecules, whereas excimer formation is not significantly affected by mesostructural changes. We propose that control of mesostructure and temperature can be a pathway toward controlling the balance between singlet fission and other competing channels.



INTRODUCTION

Organic semiconductors have the potential to enable lightweight, flexible electronic devices while at the same time reducing the energy consumption and cost in production compared to their inorganic counterparts.^{1,2} For these reasons, the use of organic photovoltaics can make so-far unused areas accessible for solar power generation.³ Critically, this requires organic photovoltaics with high efficiency under ambient conditions and evolution of this technology requires a deep understanding of the photophysics of the materials used.

The photophysics of solid organic materials can be strongly influenced by the sample temperature.^{4,5} This is due to multiple photophysically relevant properties changing upon changes in the temperature. One example is the presence of phonons, i.e., intramolecular or intermolecular vibrations, which can be activated by thermal energy.^{6,7} These vibrations facilitate intramolecular processes such as internal conversion,^{8,9} or multimolecular processes such as singlet fission,^{10,11} energy transfer^{12,13} or excimer formation.^{14,15} Also the probability of endothermic processes, in which the product has a higher energy than the educt, increases with increasing temperature.¹⁶ Another example of thermal effects are structural changes induced by temperature, which again can influence the photophysics.^{17,18}

For singlet fission, the relation between the efficiency of the process and the temperature is complex.^{10,19,20} For example,

phonons are known to play a critical role in symmetry breaking^{21,22} and energy matching of the initial singlet state and the triplet-pair state.²³ If the triplet-pair state is higher in energy than the singlet state, an increased temperature might be beneficial for singlet fission, but in this regard entropic considerations also play an important role since singlet fission doubles the number of excitations and hence increases entropy.²⁴ In solid singlet fission materials with imperfections, the occupation of trap states, which is higher at lower temperatures, can be detrimental²⁵ or beneficial^{26,27} for singlet fission, depending on the investigated system.

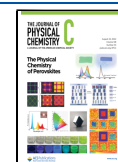
Another process that is influenced by thermal effects is excimer formation, for which the presence of facilitating phonons might help during initial formation.^{14,15} Yet, an increased temperature can also enable a pathway of thermal activation of the excimer to a more localized excited state¹⁴ and increased temperatures also increase nonluminescent excimer quenching via internal conversion.^{8,9}

Received: May 13, 2024

Revised: August 1, 2024

Accepted: August 1, 2024

Published: August 13, 2024



In the present paper, binary films containing anthradithiophene (ADT) and hexaphenylbenzene (HPhB) are investigated. ADT is chosen as main compound since it exhibits excimer formation and singlet fission as parallel multimolecular decay channels^{28,29} with intriguing temperature dependence, while we expect negligible electronic interaction between the compounds due to the high bandgap of HPhB and their low geometric similarity. Since the structural details are important for the optical properties, we shall discuss these first in some detail. Below a critical fraction of ADT of about 70%, we find limited intermixing of the two compounds, where neat HPhB phase-separates against an intimately mixed phase. We find that in this phase-separating regime, minor structural changes can be introduced by changing the compound ratio and the effect of these changes on the photophysics is analyzed by time-resolved photoluminescence (TRPL) spectroscopy. Moreover, the temperature-dependence of the TRPL properties of these differently structured samples is investigated in order to disentangle the multitude of thermal effects on the photophysics. With this approach, it is found that modifying the mixing ratio as well as changing the sample temperature are possible pathways to modify the balance between excimer formation and singlet fission.

METHODS

Previously established methods were used²⁹ and are described briefly in the following. ADT (Sigma-Aldrich, 97% purity) and HPhB (Sigma-Aldrich, 98% purity) were used as received. Hence, isomeric ADT was used, but we expect no significant effect, since both isomers, i.e., syn-ADT and anti-ADT, show similar optical and structural properties.^{28,30} The samples were prepared via codeposition (organic molecular beam deposition)³¹ in a high vacuum chamber with a base pressure of 3×10^{-8} mbar. Both compounds were resistively heated in individual Knudsen-cells. The deposition rate for each compound was monitored individually by a separate quartz crystal microbalance (QCM), calibrated to the respective compound using X-ray reflectivity (XRR) measurements. The ratio between the two compounds was named by the molar percentage of ADT in the sample. All films have a nominal thickness of 80 nm. The molecules were deposited with a total growth rate of 6 Å/min on native silicon and quartz glass substrates, which were kept at room temperature during growth. XRR measurements were performed on a General Electric XRD 3003TT instrument using $\text{CuK}\alpha_1$ radiation ($\lambda = 1.541$ Å), and grazing incidence wide-angle X-ray scattering (GIWAXS) measurements were performed on a Xeuss 2.0 (Xenocs) in-house instrument equipped with a Pilatus 300 K detector using $\text{CuK}\alpha$ radiation ($\lambda = 1.542$ Å). Absorption spectra were recorded with a PerkinElmer Lambda 950 UV-vis-NIR spectrometer. Steady-state photoluminescence (PL) measurements were performed with a LabRam HR 800 spectrometer (HORIBA Jobin Yvon, France) using a frequency-doubled Nd:YAG laser for 532 nm wavelength excitation. TRPL measurements were carried out using a synchroscan streak camera (C6860, Hamamatsu). A tunable pulsed Titanium-Sapphire laser (Tsunami, Spectra Physics) with 100 fs pulse duration and 80 MHz repetition rate was used as excitation source. The output wavelength of the laser was 960 nm and the pulses were frequency-doubled to 480 nm. The average power of the laser was attenuated to about 400 μW at the sample. The samples were mounted in a helium flow microscopy cryostat (CryoVac), where they were kept under

vacuum and cooled using liquid helium during the measurement.

RESULTS

Structural Characterization. In order to exploit the structural changes induced by intermixing of ADT with HPhB for modifications of the photoexcitation dynamics, it is, as a first step, essential to comprehend the underlying packing of the molecules. Therefore, the neat materials and binary films containing different fractions of ADT and HPhB were structurally investigated using X-ray diffraction (XRD) techniques.

For the out-of-plane structure, XRR curves of the neat and binary films are plotted in Figure 1a. Neat ADT exhibits Bragg

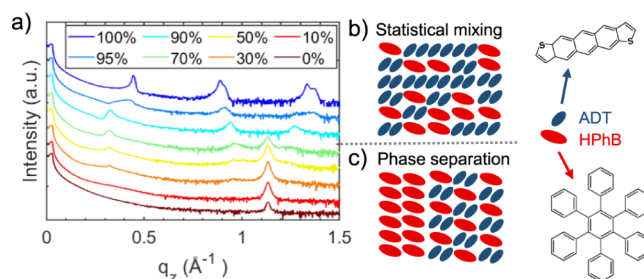


Figure 1. (a) XRR curves of neat and binary films of ADT and HPhB, plotted with a logarithmic y-axis and a vertical offset for clarity. Molar concentrations of ADT are given in the legend. (b) Schematic of the packing motif of presumed statistical mixing for ADT fractions higher than 70% and (c) schematic for presumed molecular packing in the phase separating regime. Molecular structures of both compounds are shown on the right-hand side.

peaks of first, second and third order around 0.45, 0.9, and 1.35 \AA^{-1} , respectively. Each of these peaks is split due to the coexistence of a thin film phase and a bulk phase,³² which becomes easier to see at higher Bragg peak orders. The Bragg peak positions of neat ADT are related to a d_z -spacing of around 14 Å, which indicates a standing-up orientation of the ADT molecules against the surface.³⁰

Neat HPhB exhibits only one Bragg peak at 1.14 \AA^{-1} in the displayed q_z -range, which corresponds to a d_z -spacing of 5.51 Å, corresponding to half the value of the lattice vector b of the HPhB single crystal structure.³³ Since four HPhB molecules are in each single crystal unit cell,³³ this coincidence suggests a lying-down orientation of the HPhB molecules on the substrate surface in the neat thin film.

Moving from neat ADT to binary films with high fractions of ADT, a change in peak position is found for all three Bragg peaks. Surprisingly, the peak which was assigned to the first order Bragg peak in neat ADT shifts to lower q_z -values, while the second order Bragg peak of neat ADT seems to shift to higher values. The peak, which was assigned to the third order Bragg peak of ADT, shifts to lower values again, but by a smaller amount compared to the Bragg peak at the lowest scattering vectors. Since all Bragg peaks exhibit a different shift upon adding HPhB, the second (third) order Bragg peak of ADT is not anymore at a value of two (three) times the first order Bragg peak in the binary films. As a result, the three Bragg peaks visible in the binary films with more than 70% ADT cannot be assigned to the first, second and third order anymore, suggesting a more complex out-of-plane structure of these binary films. However, a phase-separation of ADT and

HPhB can be excluded in this regime, since neither of the Bragg peak positions in the binary films agrees with the Bragg peak positions in the two neat films and since the Bragg peak positions shift continuously upon changes in the compound ratio, suggesting intermixing.^{31,34}

In the present paper, we will focus on the binary films with less than 70% ADT. In this latter region, no shifts of the Bragg peak positions can be observed. The film with 70% ADT shows four peaks, which are positioned at 0.32, 0.97, 1.13, and 1.25 \AA^{-1} . Moving from there to films with lower fractions of ADT, the peak at 1.13 \AA^{-1} gains intensity while the three other peaks gradually lose intensity until they fall below the noise level at 10% ADT. This behavior of continuous changes in peak intensity with changing compound ratio, but no changes in peak positions, suggests a phase-separation in the range of ADT fractions of approximately 70% and less.³¹ In this region, the Bragg peak at 1.13 \AA^{-1} , which is almost exactly at the position of the Bragg peak of neat HPhB, is assigned to one phase, indicating that this phase is neat HPhB. The peaks at 0.32, 0.97, and 1.25 \AA^{-1} are assigned to the other phase. These Bragg peak positions might be the same as those, toward which the Bragg peaks of the films with high fractions of ADT converge, when changing the compound ratio to 70%. Hence, this is an indication that the other phase in the phase-separating regime is a mixed phase of ADT and HPhB. The volume per molecule in the single crystal unit cell structure of HPhB³³ is almost exactly twice that of ADT.³⁰ This might be a further indication that a stable HPhB:ADT mixed phase with a ratio of 1:2 or 1:4 is possible, which would equal 66% ADT or 80% ADT, respectively. This limited intermixing model of ADT and HPhB is sketched in Figure 1c (labeled as phase-separating regime) and will be further validated by the analysis of GIWAXS data, absorption and PL spectra in the following.

After investigating the out-of-plane structure by XRR, we now turn to the in-plane structure using GIWAXS. The resulting reciprocal space maps are shown in Figure 2a. Neat ADT (subplot with 100%) shows three vertically extended diffraction features that can be assigned to the (11n), (02n) and (12n) reflections of the in-plane herringbone arrangement^{28,32} and they agree with the preferred standing-up orientation of the ADT molecules.³⁰ Moving from the neat ADT film to the binary films, these three features remain visible until they fall below the noise level at 10% ADT.

To directly compare the in-plane structure of the films, linescans along q_{xy} were extracted by integrating the GIWAXS maps in the range $0.1 \text{ \AA}^{-1} < q_z < 0.3 \text{ \AA}^{-1}$ (Figure 2b). When moving from neat ADT to the film with 70% ADT, small shifts in the q_{xy} -positions of the Bragg peaks are found, further supporting the hypothesis of intermixing in this range (see Figure 2b). Below 70% ADT, the positions of the vertically extended features do not change anymore, only the intensity decreases with decreasing fractions of ADT. At the same time, the Bragg features assignable to neat HPhB gain intensity (the most prominent one is at 1.52 \AA^{-1}). Note that the Bragg peak of the mixed phase at 1.58 \AA^{-1} overlaps with the Bragg peaks of neat HPhB at 1.52 \AA^{-1} and 1.62 \AA^{-1} , making a disentanglement of these three peaks in the phase-separating regime difficult.

Additionally, at 50% ADT and less, more localized features appear that arrange in horizontal rows at around $q_z = 0 \text{ \AA}^{-1}$, $q_z = 0.55 \text{ \AA}^{-1}$ and $q_z = 1.1 \text{ \AA}^{-1}$ (see Figure 2a). In the map with 10% ADT, the expected Bragg peak positions for the HPhB single crystal structure³³ are indicated with white crosses and

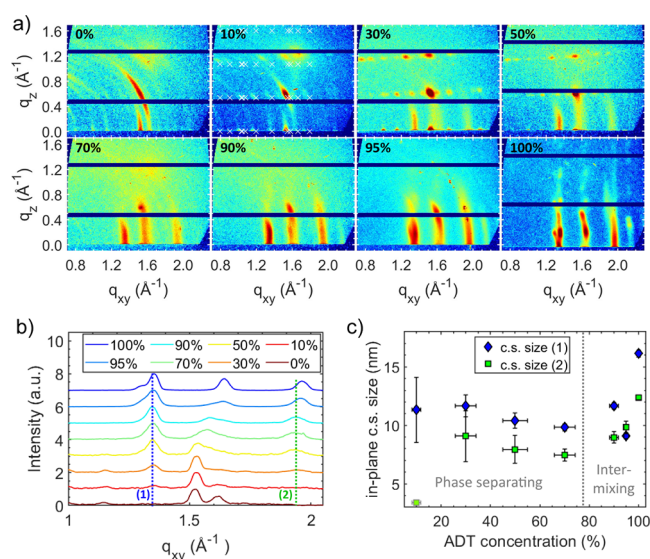


Figure 2. (a) Reciprocal space maps of neat and binary films of ADT and HPhB, indicating phase-separation below approximately 70% ADT. Molar concentrations of ADT are given in each map. In the binary film with 10% ADT, the expected Bragg peak positions based on the HPhB single crystal structure³³ are indicated with small white crosses. (b) Cross sections of the GIWAXS maps integrated along q_z in the range of $0.1 \text{ \AA}^{-1} < q_z < 0.3 \text{ \AA}^{-1}$. The peaks at 1.35 and 1.95 \AA^{-1} (best visible in the films with 70% ADT and more) are assigned to the mixed phase and named (1) and (2), respectively. (c) The widths of these peaks were used to estimate the coherently scattering size with the Scherrer equation.³⁵ The presumed regions of intermixing and phase separation are indicated in the plot. Results originating from unreliable fits are shown with faded color.

agree reasonably well with the experimentally found positions, suggesting that the localized Bragg peaks can be assigned to neat HPhB.

Neat HPhB exhibits the same Bragg peak positions, but in this case the peaks are azimuthally smeared out, making it more difficult to see and localize the features. This smearing-out indicates a less well defined orientation of the HPhB molecules in the neat film as compared to the binary films with low fractions of ADT. Note that this partial loss of preferred orientation in neat HPhB also explains why the Bragg peak of neat HPhB in the XRR data (Figure 1a) is weaker than in the binary films with low fractions of ADT.

In the present work, we are in particular interested in the phase separating regime at ADT concentrations below 70%, because this regime allows us to introduce subtle modifications of the quality of the mixed phase via tuning the compound ratio and their influence can be further addressed in optical studies. To explore these subtle changes, the Bragg peaks of the mixed phase were fitted with Gaussian functions and their widths were used to calculate the coherently scattering in-plane sizes using the Scherrer equation³⁵ (see Figure 2c). Due to the overlap with other features or due to weak peak intensity, some of the fit results have to be handled with care and the corresponding data points are plotted in faded color. For the remaining data points, a weak trend toward higher coherently scattering sizes with decreasing fractions of ADT can be found in the phase separating regime (i.e., at ADT concentrations less than 70%). This finding can be explained with the argumentation presented in ref 29, where the authors suggest a better crystallite quality of the ADT containing phase when

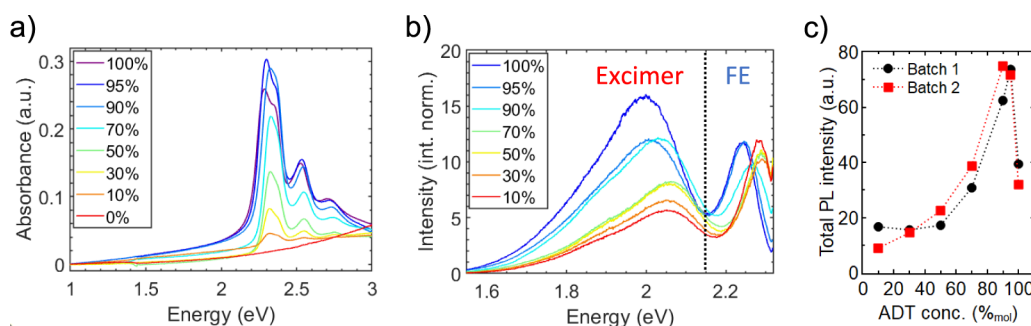


Figure 3. (a) Absorbance spectra of the neat and binary films. The curves were set to zero at 1 eV and plotted in the energy region of the $S_0 \rightarrow S_1$ transition of ADT. Significant changes in spectral shape only occur above 70% ADT, indicating limited intermixing. (b) Normalized PL spectra of neat ADT and the binary films. In order to show the relative yield of excimer emission, the spectra were normalized by the area of the free exciton (FE) peak. The photon energy of the exciting laser was 2.33 eV, which makes an excitation of HPhB impossible. For this reason, the PL spectrum of neat HPhB is omitted. (c) Spectrally integrated intensities obtained from PL measurements at two different sample positions.

the ADT concentration is reduced. This hypothesis is based on the idea that a hampered grain formation and slower growth of the ADT containing grains, which is a result of a lower ADT concentration in the film at constant total growth rates, can lead to a higher crystallite quality.^{29,31,36} Since the intensity of the Bragg peaks assigned to the mixed phase decreases with decreasing fractions of ADT, an accurate fit of the Bragg peak widths is becoming difficult at ADT fractions of 10% and below. However, based on the described growth model, it is expected that the trend of an increasing coherently scattering size with decreasing ADT fractions, which is found at higher ADT loads, continues at low ADT fractions. This is important for the understanding of the optical properties, which we shall discuss next.

Steady State Optical Spectroscopy. After having established the hypothesis of limited intermixing between ADT and HPhB based on the structural analysis, the optical properties of this system are analyzed in the following. For this purpose, absorbance spectra of the neat and binary films were recorded and are shown in Figure 3a. In the energy range below 3 eV, the $S_0 \rightarrow S_1$ transition of ADT with its vibronic progression toward higher photon energies is the only optically allowed transition, whereas HPhB with a bandgap of 5.2 eV shows only scattering (for spectra extending to higher energies including the onset of HPhB absorption, see Figure S1). In the binary films, the intensity of the ADT absorption peaks decreases with decreasing fractions of ADT. In the range of ADT concentrations above 70% ADT, also small changes in the spectral shape of the Davydov splitting including a blueshift of the entire spectrum with decreasing ADT fraction can be found. These changes can be assigned to structural changes, to which the Davydov splitting is sensitive,^{37–40} and which are induced by the admixture of HPhB, consistent with our structural analysis based on XRD. Additionally, with the admixture of the high bandgap material HPhB, the polarizability of the film decreases,⁴¹ leading to the observed increase in transition energy. Below 70% ADT, no spectral changes or shifts are found beside the decrease in overall absorbance and the Davydov splitting is present even at the lowest ADT concentration. This is in line with the idea of limited intermixing proposed in the XRD analysis.⁴² Note that, surprisingly, neat ADT does not have the highest absorption peak, which can be explained either by varying film thicknesses due to uncertainties of the QCM during film growth or by structural changes upon the admixture of HPhB. On the other hand, the admixture of HPhB might lead to structural changes

with a slightly different alignment of the transition dipole moment of the ADT molecules, which could be more favorable with regard to the incoming light compared to the neat ADT film.

All PL experiments were carried out with photon energies well below the absorption onset of HPhB, i.e., 2.33 or 2.58 eV, which means that neither excitations of HPhB nor higher electronic excitations of ADT have to be considered relevant in the analysis of the recorded PL spectra. Singlet–singlet-annihilation can also lead to higher excitations, but this process can be considered to play a negligible role for the present excitation densities, at which singlet fission and excimer formation will be shown to dominate the photophysics (see ref 29 for details). The PL spectra of neat ADT and the binary films are shown in Figure 3b. All spectra show a sharp peak around 2.25 eV and a broad peak around 2.0 eV, which both blueshift with decreasing fractions of ADT in the range of ADT concentrations of 70% and more. At concentrations below this value, the spectral position of both features does not change significantly anymore with changing ADT concentrations. As proposed in ref 28, the sharp high-energy peak is assigned to the free exciton emission and the spectrally broad peak around 2.0 eV is assigned to the excimer emission. The blueshift of the two features with decreasing ADT concentrations is assigned to changes in the polarizability of the film.²⁸ This can be rationalized following the same arguments that were given above to explain the spectral shift between the absorption spectra. Additionally, this argumentation can be used in the present case to explain why this blueshift is stronger for the excimer emission than for the free exciton emission.²⁸ In the excimer, electron and hole are predominantly localized on different molecules, thus producing a stronger dipole compared to a Frenkel exciton which predominantly resides on the same molecule. The polarization energy shift of the excimer should therefore respond more strongly to a changing polarizability of the surrounding medium.²⁸ The absence of spectral shifts at ADT concentrations below 70% once more supports limited intermixing. At ADT concentrations below this threshold, neat HPhB is expected to phase-separate from a mixed phase, which means that the addition of more HPhB does not change the local environment of the ADT molecules and hence neither the polarizability of their environment.

For normalization, the PL spectra in Figure 3b were divided by the integrated intensity (i.e., the peak area) of the ADT singlet excitons, which was determined by applying a Gaussian fit to the higher energy peak. As a result of our normalization

procedure, we find a decreasing relative contribution of the excimer luminescence with decreasing fractions of ADT. Note that while the relative contribution of the excimer peak diminishes with decreasing ADT fraction, the decay rates of the excimers are found to be similar for all investigated mixing ratios, which will be discussed in greater detail in the context of Figure 4. In the intermixing regime, this relative drop of the

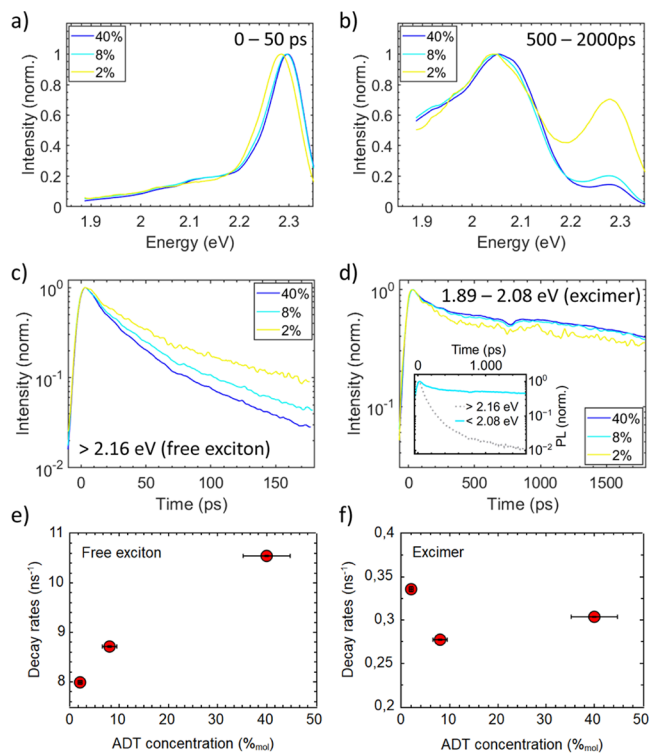


Figure 4. Spectra of binary films, extracted by time-integrating the TRPL data recorded at 200 K (a) over the first 50 ps and (b) in the time range between 500 and 2000 ps. The same data sets were used to extract decay curves of the free exciton emission in the energy range above 2.16 eV (c) and between 1.89 and 2.08 eV for the excimer emission (d). To highlight the different time scales of exciton and excimer emission, a direct comparison of both decays for the 8% mixture is shown in the subplot of panel (d). The photon energy of the exciting laser was 2.58 eV. Molar ADT concentrations of the films are given in the legends. After extracting spectra and transients, the data was noise filtered and normalized. The decay rates of the free exciton in (e) and the excimer in (f) were extracted from global biexponential fits of the data sets.

excimer intensity can be assigned to intermixing of ADT and HPhB, which reduces the amount of adjacent ADT molecules and with this the number of potential excimer sites. Additionally, a smaller number of adjacent ADT molecules should reduce the singlet fission rate. Both effects lead to a relative increase in luminescence yield of the free exciton. Notably, the relative intensity of the excimer emission does not only decrease when HPhB and ADT are intermixing (at ADT concentrations above 70%), but also in the range where additional HPhB molecules phase-separate (below 70% ADT), indicating that the addition of phase-separating HPhB can influence the photophysics of ADT. A detailed reasoning for this surprising observation will be given in the following, where we take the TRPL data into account.

The spectrally integrated PL intensities are reported in Figure 3c. While the PL intensity generally increases with

increasing ADT fraction, the neat film deviates from this trend and shows a lower overall PL intensity. This observation is surprising, but in line with the observed reduced absorption of the 100% ADT sample, in particular at the excitation energy of 2.33 eV.

Time-Resolved Spectroscopy. The molecular arrangement and hence the microstructure of the film is expected to have a significant impact on the photophysics,³⁹ especially on multimolecular processes such as singlet fission^{43–46} or excimer formation.^{47,48} Although the system investigated here shows microstructural changes in the intermixing regime (ADT concentrations above 70%), this regime of concentrations is not suitable for such an investigation for several reasons. Firstly, a significant amount of stress, strain, stacking faults and other sources of disorder are introduced into the crystallites due to the heteromolecular nature and the sample preparation procedure, which makes it challenging to extract the structural details and secondly, the statistical mixing, which is expected in the intermixing phase, implies that every ADT molecule has a slightly different local environment, which might have a comparable or even greater effect on the photophysics than the microstructural changes between two samples. Instead, the phase-separating regime of this system can be used to quantify the effects of mesostructural changes on the photophysics. For this purpose, we will in the following limit our analysis to a variation of the ADT concentration within the phase-separating regime (ADT concentrations below 70%), which means that changes in ADT concentration should mainly impact mesostructural parameters, such as the grain size, the crystallite quality or the architecture at grain boundaries.

A full representation of the TRPL data sets is provided in the Supporting Information. Spectra of the binary films were extracted from the data sets at early (0 to 50 ps) and later times (500 to 2000 ps) and are presented in Figure 4a,b, respectively. Here, we chose data recorded at 200 K, because the excimer emission was best visible in this intermediate range of temperatures. During the first 50 ps, the spectra of all films are fully dominated by the free exciton emission, which shows a slight shift to lower energies with decreasing fractions of ADT. The excimer emission is not visible during the first 50 ps, but becomes dominant after 500 ps. Similar to our observations for the steady state spectra (Figure 3b), the relative intensity of the free exciton emission after 500 ps depends on the ADT concentration, i.e., for lower ADT concentrations the relative intensity of the free exciton emission is higher.

To obtain insight into the actual decay dynamics, time traces at the energy of the free exciton emission and the excimer emission were extracted in Figure 4c,d. These decay traces clearly show that the free exciton emission decays faster than the excimer emission for all investigated samples. This is further quantified in the decay rates, which we estimated by means of global analysis (GA)⁴⁹ for the free exciton and the excimer emission in Figure 4e,f, respectively. The decay-associated spectra of the biexponential global fits are presented in Figure S7. The different spectral shapes of the fitted amplitude spectra clearly demonstrate that at 200 K the faster species can be attributed to free exciton emission, whereas the slower one represents the excimer. We would like to emphasize that our biexponential fits only serve as a rough measure for the decay dynamics, which is actually assumed to be multiexponential due to the presence of spatial and energetic

disorder. Thus, the fitted decay times will always depend on the observed time window. Nevertheless, our fits represent a simple approach to capture the decay dynamics of the free exciton and excimer populations and to compare the dynamics for different mixing ratios. In case of the free exciton emission, an acceleration of the decay with increasing fractions of ADT can be found, while the decay rates of the excimer emission are comparable for all samples.

Temperature Effects. To explore the influence of temperature on the exciton dynamics, we carried out temperature dependent measurements, covering a broad range from 10 K to room temperature. Temperature dependent PL spectra, which were integrated over the entire time range of the measurement (0 to 2000 ps), are presented in Figure 5a–c.

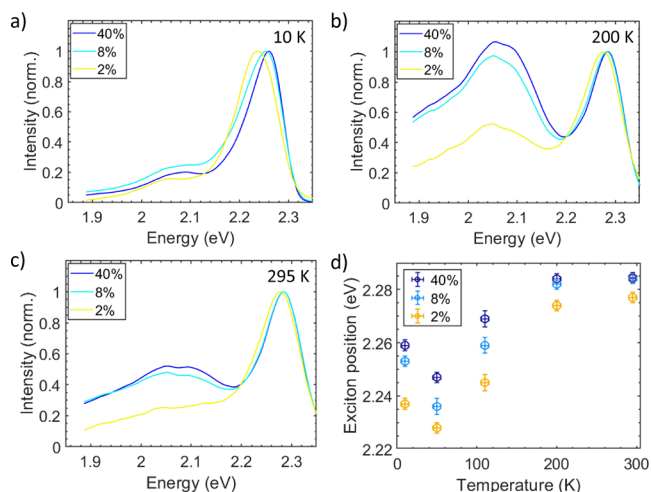


Figure 5. Spectra of binary films in (a–c) were extracted by time-integrating the TRPL data recorded at different sample temperatures from 0 to 2000 ps and noise filtering the resulting spectra before normalizing them with respect to the free exciton emission. The photon energy of the exciting laser was 2.58 eV. Molar ADT concentrations of the films are given in the legends and the sample temperature is given inside each plot. Panel (d) summarizes the energies of the free exciton peaks extracted for different ADT concentrations and different temperatures. The vertical errors given equal 2% of the fwhm, the horizontal errors equal 5 K.

In all spectra except for the 40% ADT sample at 200 K, the free exciton emission is the dominant contribution and at all temperatures the free exciton emission is shifting to the red when the ADT concentration is reduced, which contrasts with the findings made for the high ADT concentrations in the intermixing regime. The plot of the free exciton peak energies in Figure 5d demonstrates that this shift between the samples is more pronounced at lower temperatures.

At temperatures of 110 K and higher, excimer emission is clearly visible for all ADT concentrations, as further justified by the emission spectra provided in Figure S8. At lower temperatures, the intensity of the excimer emission decreases to a point, where it cannot be clearly disentangled from the vibronic progression of the free exciton emission anymore, which is expected to peak around 2.1 eV.²⁹ Interestingly, there is no monotonic trend in the relative intensity of the excimer emission. While it gains intensity upon reducing the temperature from room temperature to 200 K, the relative intensity

decreases again when moving to even lower temperatures, consistent with our observations in ref 50.

For each sample, time traces of the short-lived higher-energetic emission and the long-lived emission at lower energies were extracted at different temperatures. Exemplary data for the sample with 8% ADT are presented in Figure 6a,b,

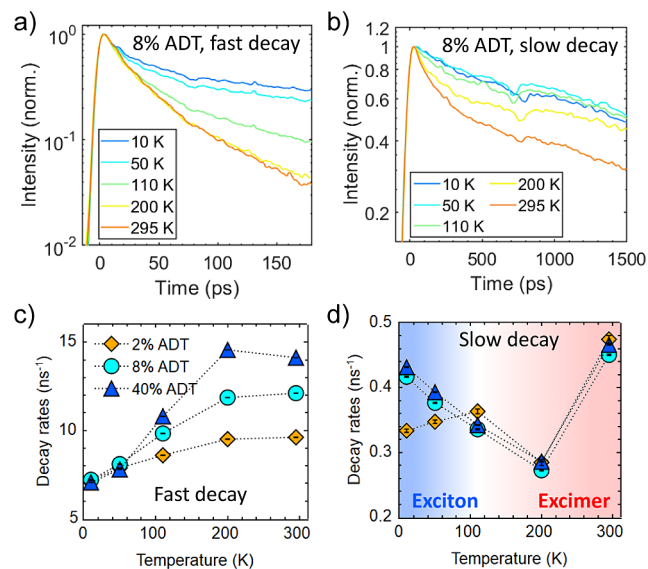


Figure 6. Decay traces extracted from the energy range of the free exciton emission above 2.16 eV for the sample with 8% ADT are presented in (a). The excimer decay traces of the same sample at different temperatures in (b) are averaged over an energy range from 1.89 to 2.08 eV. The photon energy of the exciting laser was 2.58 eV. The sample temperatures are given in the legend. Panel (c) summarizes the fast decay rates extracted from global biexponential fits of the data sets, which can be attributed to free exciton decay. The decay rates in (d) were extracted from global biexponential fits of the energy range below 2.08 eV, in order to be more sensitive to the excimer emission.

whereas similar trends are found for the other ADT concentrations (see Figures S9 and S10). Based on the foregoing discussion, the emission signature at higher energies can be fully attributed to free exciton emission. The feature at lower emission energies on the other hand represents excimer decay at elevated temperatures, whereas at temperatures below 110 K the decay is governed by longer-lived emission from the exciton state. To further quantify the underlying temperature-dependent dynamics, we applied the global biexponential fitting routine introduced above to the temperature dependent data sets. The corresponding decay associated spectra are presented in Figure S7 and they give further support for the different origins of the longer-lived decay at temperatures below and above 110 K. The decay rates obtained for the fast and the slow component are summarized in Figure 6c,d, respectively. In order to be more sensitive to excimer emission, only the energy range below 2.08 eV was fitted and the longer-lived component from the biexponential fits is displayed.

At low temperatures, all investigated compositions show similar fast decay rates. Similarities also arise regarding the onset of a faster process, which occurs in a temperature range between 100 and 200 K for all compositions. On the other hand, there is a clear compositional dependence in this short-lived species at higher temperatures with higher ADT fractions leading to faster decay. This is expected for an endothermic

singlet fission process, as further detailed in the discussion section.

The more intricate trends observed for the slower fitted species can be understood by considering its different origins, which is also highlighted by the colors in Figure 6d. The decay at temperatures below 110 K originates from a superposition of excimer emission and longer-lived exciton decay. Except for the sample with the lowest ADT concentration, this long decay component slows further down with increasing temperature until a range of intermediate temperatures around 110 K is reached. This decrease in decay rates likely originates from the onset of slower excimer emission. As observed from the spectra, the excimer signature becomes dominant in the longer time range at temperatures of 200 K and above, suggesting that in this regime our fit captures the excimer dynamics. The analysis reveals an acceleration of the decay dynamics when the temperature increases further to room temperature, but notably, there is no apparent compositional dependence of the excimer decay.

DISCUSSION

Structural Effects. First of all, the clear changes in free exciton decay rate with changing ADT concentrations in the phase separating regime are an intriguing result, since it is not expected that adding phase-separated grains of a different material can have a significant impact on the dominant decay channel of ADT excitons, which is singlet fission.²⁹ This observation can potentially be explained in the following way. We propose a model in which it is, for simplicity, assumed that the mixed phase has an ADT:HPhB stoichiometry of 2:1, as schematically illustrated in Figure 1c, but the explanation would work equally well for stoichiometries different from 2:1. As Figure 2c indicates, the coherently scattering size of the mixed phase in the phase separating regime increases with decreasing fractions of ADT, implying that the mixed crystallites are better ordered at low fractions of ADT. One possible parameter of better order would be a transition from statistical intermixing to a regularly ordered cocrystal. We can use the simple 2D model presented in Figure 1b,c to qualitatively illustrate the differences between the different mixing scenarios. For a 2:1 stoichiometry, every ADT molecule has exactly one directly neighboring ADT molecule in-plane (Figure 1b), whereas in a statistical mixing scenario an ADT molecule can have between zero and four direct ADT neighbors in plane, with a statistical average of 2.66 direct neighbors (Figure 1c). This average number of next neighbors is higher than for the cocrystal phase. Note that the number 2.66 is the number of in-plane neighboring sites (4) multiplied with the ADT concentration (66%).⁵¹ Now, the higher average number in the statistically mixed case compared to the cocrystal would explain the higher singlet fission rate at higher fractions of ADT. This is the case because ADT exhibits incoherent singlet fission,²⁸ the rate of which linearly increases with the number of nearest neighbors of the same kind.⁵² Note that many other common explanations for the decrease in singlet fission rates with decreasing ADT concentrations can be ruled out. An assignment of the slow-down of singlet fission to a higher density of trap states is not in line with the proposed higher crystallite quality at low ADT concentrations. Also, an assignment of the decreased decay rates to ADT molecules incorporated into HPhB crystallites is not possible, since these molecules would experience an environment of lower polarizability. This would lead to a significant blueshift of the free

exciton emission peak with decreasing fractions of ADT, which is, however, not observed. With the same argument it can also be excluded that the slow-down is due to changes in the stoichiometry of the mixed phase, since then once again a change in polarizability and hence energy of the free exciton would be observed.

Now, after discussing the decay of the free exciton, the excimer emission is investigated. GA of the decay rates did not show any compositional dependence of the slow decay rates at elevated temperatures (Figures 4f and 6), suggesting that the addition of phase-separating HPhB has no strong effect on the excimer decay dynamics. However, another question of interest is, whether the formation of excimers is actually altered by variations of the molecular packing. Although the time resolution of the TRPL setup is insufficient to track the excimer formation (typical time scales are 200 fs^{53–55}) some insight into the formation dynamics can be gained by analyzing the relative intensities of the PL signatures. The ratio between the initial intensities of the free exciton emission A_0^{FE} and the excimer emission A_0^{ex} is a measure for the amount of excimers created per free singlet exciton. Due to the overlapping signatures, analyzing these amplitudes directly would be rather inaccurate, therefore we utilize the fitted decay rates k^{FE} , k^{ex} and the overall steady state intensity of the excimer emission I_{ss}^{ex} , exploiting the interrelation

$$\frac{A_0^{ex}}{A_0^{FE}} \propto I_{ss}^{ex} \frac{k^{ex}}{k^{FE}} \quad (1)$$

which allows us to renormalize the spectra extracted in Figure 5b. Details of this procedure and resulting spectra are given in the Supporting Information. After multiplying the normalized spectra in Figure 5b with the ratio of decay rates $\frac{k^{ex}}{k^{FE}}$, we obtain a representation of intensities proportional to the excimer formation yield (see Figure S11). Importantly, similar intensities of the excimer emission after this normalization procedure suggest that the yield of excimer formation is actually similar in all samples and thus the strong changes in the intensity ratio of free exciton and excimer emission can be mainly assigned to changes in the singlet fission rate with changing ADT concentration. These results agree with the perception that the singlet fission rate in ADT depends on the number of nearest neighbors of the same kind,²⁸ while the excimer formation rate seems to be equally fast, as soon as at least one adjacent ADT molecule is present.

Temperature Effects. In the following, the temperature dependence of the emission spectra is discussed. Regarding the peak positions extracted for the free exciton emission in Figure 5, we find a redshift of the free exciton peak with decreasing temperatures, which, however, changes to a blueshift when moving from 50 K to the lowest temperature of 10 K. Temperature dependent shifts of the emission energy can have several origins, such as variations of intermolecular or interatomic equilibrium distances, phase transitions or variations in the population of vibronically excited states. However, here, the observed blueshift of the emission energy at very low temperatures is a strong indication for the presence of localized states, which are potentially responsible for the observed peak shifts in the overall temperature range, as explained in the following. Assuming a Gaussian distribution of the density of states in energy, free excitons can perform a hopping transport between individual states. Higher temper-

atures will allow for thermally activated hopping transport, i.e., excitons can also be thermally excited into states with slightly higher energies, such that for higher temperatures a blue-shift of the emission maximum is expected. When the temperature is reduced, thermally activated hopping events become less frequent and it is more likely that excitons relax into sites with lower energy. In this regime, thermal activation may still increase the transport distances of excitons, enabling them to reach states which are even lower in energy. However, in disordered systems, this transport mechanism can become kinetically frustrated for even lower temperatures, such that excitons populate local minima in the density of states. In these tail states, they are spatially isolated from other low-energetic sites, such that they cannot relax further without overcoming significant energetic barriers. Compared to the situation where little thermal energy is available to help the excitons to relax further, a blueshift is expected when going to the lowest range of temperatures.¹³ This mechanism can explain why the energetic position of the free exciton emission is higher at 10 K than at 50 K. The fact that the energetic position of the free exciton emission is lower for samples with lower fractions of ADT at all temperatures actually suggests that there are more low-energetic trap sites for the sample with the lowest ADT fraction. This assumption could also give an explanation why the differences between the samples are more pronounced at lower temperatures, because in this regime, only lower energetic sites are populated due to a lack of thermal energy and hence the density of localized states has a more influential role.

The finding of a presumably higher density of lower-energetic trap states at lower ADT-concentrations is counter-intuitive, because on the other hand we have found an increase of the coherently scattering size of the mixed phase (see Figure 2c). Although the existence of trap sites as a result of energetic disorder might reduce the coherently scattering size, another important factor is lattice strain. In the statistically mixed case, which is present at higher ADT fractions, the lattice stress is higher due to geometric differences between the molecules, decreasing the coherently scattering size. In contrast, the regular molecular arrangement in a cocrystal reduces lattice stress and hence increases the coherently scattering size. This effect of strain on the coherently scattering size might overcompensate the effect of trap sites. Moreover, even though we cannot make a definite statement about the nature of the trap states, it is reasonable to assume that packing faults associated with energetic disorder could emerge in particular at the boundaries between the mixed phase and the pure HPhB phase.

Lastly, the temperature dependent PL dynamics in Figure 6 will be discussed and connected to the peculiar temperature dependencies of the emission spectra presented in Figure 5. For the free exciton emission, we observe a remarkable decrease of the decay rate when the temperature decreases below 200 K. Since nonradiative singlet fission is assumed to be the dominating decay channel in ADT, it is reasonable to consider that singlet fission in this material is a thermally activated process. This appears to be counterintuitive, because the energy of the ¹(TT) state is below the energy of the exciton in ADT,^{56,57} meaning that triplet-pair formation in ADT should in principle be exothermic. However, the overall process could still be thermally activated, e.g., due to thermally activated hopping into sites with more adjacent ADT molecules, where singlet fission is more favorable.^{37,50} For

the excimer emission, we find an increase of the relative intensity and a decrease of the decay rates, when cooling the sample to intermediate temperatures around 200 K. Similar as for the free excitons, this is indicative for a nonradiative channel, for which it is generally expected that its efficiency decreases with decreasing temperatures.^{8,9} It is likely, that this nonradiative process in case of the excimer is actually a nonradiative transition back to the electronic ground state, since an excimer deactivation pathway by thermal activation from the excimer to the exciton, followed by singlet fission can be considered to have negligible impact in the investigated temperature range, as demonstrated in the Supporting Information. It is also noteworthy that at 200 K and above, where quantitative analysis of the excimer emission is possible, the yield of excimers formed per singlet exciton, which can be analyzed by eq 1, does not change notably (see Figure S11 for details), suggesting that the process is fully activated at 200 K. This gives further support for the statement that the decrease of the relative intensity with increasing temperature is indeed caused by nonradiative decay. Moving to temperatures lower than 200 K, it becomes challenging to make quantitative statements about the excimer emission, as the relative oscillator strength drops and the emission gets more and more superimposed by longer lived free exciton decay. This finding suggests, that excimer formation at low temperatures is rather suppressed, which is similar to observations made for perylene,^{14,15} where relaxation into the excimer state was inhibited at low temperatures, potentially due to the absence of vibronic excitations, which are needed to drive the process.

CONCLUSION

In the present work, we have investigated the photophysics of ADT in blends with the structurally different high-bandgap compound HPhB. For concentrations of ADT above approximately 70%, we have identified an intermixing regime, where structural and optical parameters can be continuously tuned via the ADT fraction. Below 70% ADT on the other hand, a phase separating regime with a mixed phase and a neat HPhB phase emerges. Surprisingly, this phase separating regime shows improved crystal quality, i.e., a higher coherently scattering size of the mixed phase with decreasing ADT fraction, which was attributed to a slower and more controlled growth of the ADT-rich domains in an environment where less ADT molecules are provided. In this phase, we also found unexpected trends in the photoexcitation dynamics, i.e., a slow-down of singlet fission with decreasing fractions of ADT. This result was explained by the transition of the mixed phase from solid-solution to cocrystal with decreasing fractions of ADT, which increases the coherently scattering size. On the other hand, this transition decreases the number of nearest ADT neighbors of the same kind, which likely causes the decrease of the incoherent singlet fission rate of ADT.^{28,52} The formation of excimers on the subpicosecond time scale, on the other hand, seems to be rather unaffected by the mixing ratio. We find that the relative decrease of the excimer emission with decreasing ADT fraction rather originates from the increasing contribution of singlet exciton emission due to diminishing singlet fission.

We have also analyzed the temperature-dependence of the photophysics in the phase separating regime. In agreement with earlier reports, we find that singlet fission is thermally activated, leading to concentration-independent dynamics of free excitons at low temperatures and concentration-dependent

accelerated dynamics at elevated temperatures. Pronounced longer-lived dynamics, which can be unambiguously attributed to excimer emission, is only observed at temperatures above approximately 110 K, supporting the view that excimer formation is an activated process. Beside the intrinsic kinetics, temperature-dependent studies have also provided insight into the presence of energetic disorder. We have hypothesized that in the low temperature regime spectral shifts with temperature are caused by energy transfer of excitons to lower-energetic tail states with thermal energy enabling hopping transport between these sites and kinetic frustration at the lowest temperatures.

With our findings, we have demonstrated that both, mesostructural modifications as well as tuning of the temperature, induce changes of the photophysics of binary molecular systems, i.e., they influence the balance between singlet fission and excimer formation. Combining structural and time-resolved optical studies is a powerful approach to comprehensively study the interrelation between photophysics and molecular packing. Understanding the underlying photophysics is eventually an important prerequisite to tailor new devices based on molecular blends.

■ ASSOCIATED CONTENT

SI Supporting Information

The Supporting Information is available free of charge at <https://pubs.acs.org/doi/10.1021/acs.jpcc.4c03155>.

Absorbance spectra at higher energies, color maps of the recorded TRPL data, supporting data for global analysis, temperature-dependent PL spectra and decay curves, estimation of excimers created per singlet exciton, and calculation of the thermal activation of excimers in ADT back to the singlet state (PDF)

■ AUTHOR INFORMATION

Corresponding Authors

Marina Gerhard – Faculty of Physics and Material Sciences Centre, Philipps-Universität Marburg, Marburg 35032, Germany; orcid.org/0000-0002-6539-4675; Email: marina.gerhard@physik.uni-marburg.de

Frank Schreiber – Institut für Angewandte Physik, Universität Tübingen, Tübingen 72076, Germany; orcid.org/0000-0003-3659-6718; Email: frank.schreiber@uni-tuebingen.de

Authors

Julian Hausch – Institut für Angewandte Physik, Universität Tübingen, Tübingen 72076, Germany; orcid.org/0000-0002-8033-2771

Nico Hofeditz – Faculty of Physics and Material Sciences Centre, Philipps-Universität Marburg, Marburg 35032, Germany; orcid.org/0000-0001-6954-5779

Jona Bredehöft – Institut für Angewandte Physik, Universität Tübingen, Tübingen 72076, Germany

Katharina Broch – Institut für Angewandte Physik, Universität Tübingen, Tübingen 72076, Germany

Complete contact information is available at: <https://pubs.acs.org/doi/10.1021/acs.jpcc.4c03155>

Notes

The authors declare no competing financial interest.

■ ACKNOWLEDGMENTS

J.H., K.B., and F.S. acknowledge funding by the German Research Foundation (BR4869/4-1 and SCHR700/38-1, respectively). N.H. and M.G. acknowledge funding by the German Research Foundation in the framework of SFB 1083 (Subproject B10 – No. 223848855). Moreover, the authors thank Prof. Martin Koch for providing access to experimental setups for time-resolved PL spectroscopy.

■ REFERENCES

- (1) Smith, M. B.; Michl, J. Recent advances in singlet fission. *Annu. Rev. Phys. Chem.* **2013**, *64*, 361–386.
- (2) Smith, M. B.; Michl, J. Singlet fission. *Chem. Rev.* **2010**, *110*, 6891–6936.
- (3) Pagliaro, M.; Ciriminna, R.; Palmisano, G. Flexible solar cells. *ChemSuschem* **2008**, *1*, 880–891.
- (4) Brütting, W. *Physics of organic semiconductors*; Wiley VCH: Weinheim, 2005.
- (5) Clark, J.; Silva, C.; Friend, R. H.; Spano, F. C. Role of intermolecular coupling in the photophysics of disordered organic semiconductors: aggregate emission in regioregular polythiophene. *Phys. Rev. Lett.* **2007**, *98*, 206406.
- (6) Gierschner, J.; Mack, H.-G.; Lüer, L.; Oelkrug, D. Fluorescence and absorption spectra of oligophenylenevinyls: Vibronic coupling, band shapes, and solvatochromism. *J. Chem. Phys.* **2002**, *116*, 8596–8609.
- (7) Wu, C. C.; Korovyanko, O. J.; Delong, M. C.; Vardeny, Z. V.; Ferraris, J. P. Optical studies of distyrylbenzene single crystals. *Synth. Met.* **2003**, *139*, 735–738.
- (8) Zhang, M.; Wang, W.; Yin, S.; Meng, R.; Li, C.; Gao, K. Temperature effect on the internal conversion dynamics following different stimulated absorptions in a conjugated polymer. *Org. Electron.* **2018**, *56*, 201–207.
- (9) Litvinenko, K. L.; Webber, N. M.; Meech, S. R. Internal conversion in the chromophore of the green fluorescent protein: temperature dependence and isoviscosity analysis. *J. Phys. Chem. A* **2003**, *107*, 2616–2623.
- (10) Tamura, H.; Huix-Rotllant, M.; Burghardt, I.; Olivier, Y.; Beljonne, D. First-principles quantum dynamics of singlet fission: Coherent versus thermally activated mechanisms governed by molecular π stacking. *Phys. Rev. Lett.* **2015**, *115*, 107401.
- (11) Miyata, K.; Kurashige, Y.; Watanabe, K.; Sugimoto, T.; Takahashi, S.; Tanaka, S.; Takeya, J.; Yanai, T.; Matsumoto, Y. Coherent singlet fission activated by symmetry breaking. *Nat. Chem.* **2017**, *9*, 983–989.
- (12) Mikhnenko, O. V.; Blom, P. W. M.; Nguyen, T.-Q. Exciton diffusion in organic semiconductors. *Energy Environ. Sci.* **2015**, *8*, 1867–1888.
- (13) Athanasopoulos, S.; Hoffmann, S. T.; Bäessler, H.; Köhler, A.; Beljonne, D. To hop or not to hop? Understanding the temperature dependence of spectral diffusion in organic semiconductors. *J. Phys. Chem. Lett.* **2013**, *4*, 1694–1700.
- (14) Seyfang, R.; Port, H.; Wolf, H. C. Picosecond study on excimer formation in pyrene single crystals II. The excimer precursor state in the high-temperature phase. *J. Lumin.* **1988**, *42*, 127–135.
- (15) Walker, B.; Port, H.; Wolf, H. C. The two-step excimer formation in perylene crystals. *Chem. Phys.* **1985**, *92*, 177–185.
- (16) Kaiser, C.; Sandberg, O. J.; Zarrabi, N.; Li, W.; Meredith, P.; Armin, A. A universal Urbach rule for disordered organic semiconductors. *Nat. Commun.* **2021**, *12*, 3988.
- (17) Hammer, S.; Ferschke, T.; Eyb, G.; Pflaum, J. Phase transition induced spectral tuning of dual luminescent crystalline zinc-phthalocyanine thin films and OLEDs. *Appl. Phys. Lett.* **2019**, *115*, 263303.
- (18) Cölle, M.; Brütting, W. Thermal, structural and photophysical properties of the organic semiconductor Alq₃. *Phys. Status Solidi A* **2004**, *201*, 1095–1115.

- (19) Burdett, J. J.; Gosztola, D.; Bardeen, C. J. The dependence of singlet exciton relaxation on excitation density and temperature in polycrystalline tetracene thin films: Kinetic evidence for a dark intermediate state and implications for singlet fission. *J. Chem. Phys.* **2011**, *135*, 214508.
- (20) Cruz, C. D.; Chronister, E. L.; Bardeen, C. J. Using temperature dependent fluorescence to evaluate singlet fission pathways in tetracene single crystals. *J. Chem. Phys.* **2020**, *153*, 234504.
- (21) Xie, X.; Santana-Bonilla, A.; Fang, W.; Liu, C.; Troisi, A.; Ma, H. Exciton-phonon interaction model for singlet fission in prototypical molecular crystals. *J. Chem. Theory Comput.* **2019**, *15*, 3721–3729.
- (22) Tao, G. Bath effect in singlet fission dynamics. *J. Phys. Chem. C* **2014**, *118*, 27258–27264.
- (23) Unger, F.; Moretti, L.; Hausch, J.; Bredehoeft, J.; Zeiser, C.; Haug, S.; Tempelaar, R.; Hestand, N. J.; Cerullo, G.; Broch, K. Modulating singlet fission by scanning through vibronic resonances in pentacene-based blends. *J. Am. Chem. Soc.* **2022**, *144*, 20610–20619.
- (24) Chan, W.-L.; Ligges, M.; Zhu, X.-Y. The energy barrier in singlet fission can be overcome through coherent coupling and entropic gain. *Nat. Chem.* **2012**, *4*, 840–845.
- (25) Mayonado, G.; Vogt, K. T.; Van Schenck, J. D. B.; Zhu, L.; Fregoso, G.; Anthony, J.; Ostroverkhova, O.; Graham, M. W. High-symmetry anthradithiophene molecular packing motifs promote thermally activated singlet fission. *J. Phys. Chem. C* **2022**, *126*, 4433–4445.
- (26) Tao, G. Energy fluctuations induced quantum decoherence and exciton localization in singlet fission. *J. Phys. Chem. C* **2019**, *123*, 29571–29579.
- (27) Piland, G. B.; Bardeen, C. J. How morphology affects singlet fission in crystalline tetracene. *J. Phys. Chem. Lett.* **2015**, *6*, 1841–1846.
- (28) Hausch, J.; Berges, A. J.; Zeiser, C.; Rammner, T.; Morlok, A.; Bredehoeft, J.; Hammer, S.; Pflaum, J.; Bardeen, C. J.; Broch, K. Distinguishing between triplet-pair state and excimer emission in singlet fission chromophores using mixed thin films. *J. Phys. Chem. C* **2022**, *126*, 6686–6693.
- (29) Hausch, J.; Hofeditz, N.; Bredehoeft, J.; Hammer, S.; Pflaum, J.; Broch, K.; Gerhard, M.; Schreiber, F. Influence of excited-state delocalization on singlet fission: tuning triplet-pair-state emission in thin films. *J. Phys. Chem. C* **2023**, *127*, 3778–3786.
- (30) Mamada, M.; Katagiri, H.; Mizukami, M.; Honda, K.; Minamiki, T.; Teraoka, R.; Uemura, T.; Tokito, S. Syn-/anti-anthradithiophene derivative isomer effects on semiconducting properties. *ACS Appl. Mater. Interfaces* **2013**, *5*, 9670–9677.
- (31) Hinderhofer, A.; Schreiber, F. Organic-organic heterostructures: Concepts and applications. *ChemPhysChem* **2012**, *13*, 628–643.
- (32) Wang, C.-H.; Jian, S.-D.; Chan, S.-W.; Ku, C.-S.; Huang, P.-Y.; Chen, M.-C.; Yang, Y.-W. Enhanced stability of organic field-effect transistors with blend pentacene/anthradithiophene films. *J. Phys. Chem. C* **2012**, *116*, 1225–1231.
- (33) Bart, J. C. J. The crystal structure of a modification of hexaphenylbenzene. *Acta Crystallogr.* **1968**, *24*, 1277–1287.
- (34) Aufderheide, A.; Broch, K.; Novák, J.; Hinderhofer, A.; Nervo, R.; Gerlach, A.; Banerjee, R.; Schreiber, F. Mixing-induced anisotropic correlations in molecular crystalline systems. *Phys. Rev. Lett.* **2012**, *109*, 156102.
- (35) Patterson, A. L. The Scherrer formula for X-ray particle size determination. *Phys. Rev.* **1939**, *56*, 978–982.
- (36) Andreasson, M.; Ilver, L.; Kanski, J.; Andersson, T. G. Organic molecular beam deposition system and initial studies of organic layer growth. *Phys. Scr.* **2006**, *2006*, 1.
- (37) Broch, K.; Dieterle, J.; Branchi, F.; Hestand, N. J.; Olivier, Y.; Tamura, H.; Cruz, C.; Nichols, V. M.; Hinderhofer, A.; Beljonne, D.; et al. Robust singlet fission in pentacene thin films with tuned charge transfer interactions. *Nat. Commun.* **2018**, *9*, 954.
- (38) Davydov, A. S. The theory of molecular excitons. *Sov. Phys. Uspekhi* **1964**, *7*, 145.
- (39) Tanaka, S.; Miyata, K.; Sugimoto, T.; Watanabe, K.; Uemura, T.; Takeya, J.; Matsumoto, Y. Enhancement of the exciton coherence size in organic semiconductor by alkyl chain substitution. *J. Phys. Chem. C* **2016**, *120*, 7941–7948.
- (40) Yamagata, H.; Norton, J.; Hontz, E.; Olivier, Y.; Beljonne, D.; Brédas, J. L.; Silbey, R. J.; Spano, F. C. The nature of singlet excitons in oligoacene molecular crystals. *J. Chem. Phys.* **2011**, *134*, 204703.
- (41) Hervé, P.; Vandamme, L. K. J. General relation between refractive index and energy gap in semiconductors. *Infrared Phys. Technol.* **1994**, *35*, 609–615.
- (42) Theurer, C. P.; Valencia, A. M.; Hausch, J.; Zeiser, C.; Sivanesan, V.; Cocchi, C.; Tegeder, P.; Broch, K. Photophysics of charge transfer complexes formed by tetracene and strong acceptors. *J. Phys. Chem. C* **2021**, *125*, 6313–6323.
- (43) Tom, R.; Gao, S.; Yang, Y.; Zhao, K.; Bier, I.; Buchanan, E. A.; Zaykov, A.; Havlas, Z.; Michl, J.; Marom, N. Inverse design of tetracene polymorphs with enhanced singlet fission performance by property-based genetic algorithm optimization. *Chem. Mater.* **2023**, *35*, 1373–1386.
- (44) Pensack, R. D.; Tilley, A. J.; Grieco, C.; Purdum, G. E.; Ostroumov, E. E.; Granger, D. B.; Oblinsky, D. G.; Dean, J. C.; Doucette, G. S.; Asbury, J. B.; et al. Striking the right balance of intermolecular coupling for high-efficiency singlet fission. *Chem. Sci.* **2018**, *9*, 6240–6259.
- (45) Dillon, R. J.; Piland, G. B.; Bardeen, C. J. Different rates of singlet fission in monoclinic versus orthorhombic crystal forms of diphenylhexatriene. *J. Am. Chem. Soc.* **2013**, *135*, 17278–17281.
- (46) Aster, A.; Zinna, F.; Rumble, C.; Lacour, J.; Vauthey, E. Singlet fission in a flexible bichromophore with structural and dynamic control. *J. Am. Chem. Soc.* **2021**, *143*, 2361–2371.
- (47) Gao, Y.; Liu, H.; Zhang, S.; Gu, Q.; Shen, Y.; Ge, Y.; Yang, B. Excimer formation and evolution of excited state properties in discrete dimeric stacking of an anthracene derivative: A computational investigation. *Phys. Chem. Chem. Phys.* **2018**, *20*, 12129–12137.
- (48) Aster, A.; Licari, G.; Zinna, F.; Brun, E.; Kumpulainen, T.; Tajkhorshid, E.; Lacour, J.; Vauthey, E. Tuning symmetry breaking charge separation in perylene bichromophores by conformational control. *Chem. Sci.* **2019**, *10*, 10629–10639.
- (49) Snellenburg, J. J.; Laptinok, S.; Seger, R.; Mullen, K. M.; van Stokkum, I. H. M. Glotaran: A Java-based graphical user interface for the R package TIMP. *J. Stat. Software* **2012**, *49*, 1–22.
- (50) Hofeditz, N.; Hausch, J.; Broch, K.; Heimbrot, W.; Schreiber, F.; Gerhard, M. Efficient energy transfer and singlet fission in co-deposited thin films of pentacene and anthradithiophene. *Adv. Mater. Interfaces* **2024**, *11*, 2300922.
- (51) Zeiser, C. F. *Controlled variation of intermolecular coupling in polycrystalline thin films of singlet fission chromophores*, Ph.D. thesis, Universität Tübingen, 2021.
- (52) Zeiser, C.; Cruz, C.; Reichman, D. R.; Seitz, M.; Hagenlocher, J.; Chronister, E. L.; Bardeen, C. J.; Tempelaar, R.; Broch, K. Vacancy control in acene blends links exothermic singlet fission to coherence. *Nat. Commun.* **2021**, *12*, 5149.
- (53) Sung, J.; Kim, P.; Fimmel, B.; Würthner, F.; Kim, D. Direct observation of ultrafast coherent exciton dynamics in helical π -stacks of self-assembled perylene bisimides. *Nat. Commun.* **2015**, *6*, 8646.
- (54) Kaufmann, C.; Kim, W.; Nowak-Król, A.; Hong, Y.; Kim, D.; Würthner, F. Ultrafast exciton delocalization, localization, and excimer formation dynamics in a highly defined perylene bisimide quadruple π -stack. *J. Am. Chem. Soc.* **2018**, *140*, 4253–4258.
- (55) Hong, Y.; Kim, W.; Kim, T.; Kaufmann, C.; Kim, H.; Würthner, F.; Kim, D. Real-time observation of structural dynamics triggering excimer formation in a perylene bisimide folda-dimer by ultrafast time-domain raman spectroscopy. *Angew. Chem., Int. Ed.* **2022**, *61*, No. e202114474.
- (56) Yong, C. K.; Musser, A. J.; Bayliss, S. L.; Lukman, S.; Tamura, H.; Bubnova, O.; Hallani, R. K.; Meneau, A.; Resel, R.; Maruyama, M.; et al. The entangled triplet pair state in acene and heteroacene materials. *Nat. Commun.* **2017**, *8*, 15953.

(57) Bossanyi, D. G.; Matthiesen, M.; Wang, S.; Smith, J. A.; Kilbride, R. C.; Shipp, J. D.; Chekulaev, D.; Holland, E.; Anthony, J. E.; Zaumseil, J.; et al. Emissive spin-0 triplet-pairs are a direct product of triplet–triplet annihilation in pentacene single crystals and anthradithiophene films. *Nat. Chem* **2021**, *13*, 163–171.